

# Characterization and monitoring of tool wear in ultrasonic metal welding

Chenhui Shao<sup>1,#</sup>, Weihong Guo<sup>2</sup>, Tae H. Kim<sup>1</sup>, Jionghua (Judy) Jin<sup>2</sup>, S. Jack Hu<sup>1,2</sup>, J. Patrick Spicer<sup>3</sup>, and Jeffrey A. Abell<sup>3</sup>

<sup>1</sup> Department of Mechanical Engineering, University of Michigan, Ann Arbor, MI, USA

<sup>2</sup> Department of Industrial and Operations Engineering, University of Michigan, Ann Arbor, MI, USA

<sup>3</sup> Manufacturing Systems Research Lab, General Motors Technical Center, Warren, MI, USA

# Corresponding Author / E-mail: chshao@umich.edu

KEYWORDS : Tool wear characterization , Tool wear monitoring, Ultrasonic metal welding

*This paper presents some preliminary results in characterizing, understanding and monitoring tool wear in micro ultrasonic metal welding, which has recently been adopted for lithium-ion battery manufacturing. As a result of a lack of effective tool condition monitoring (TCM) systems, tool replacement, including horn and anvil, constitutes a major part of the production costs. But it is very challenging to accurately identify tool conditions and develop TCM systems due to the complexity of the process mechanism and tool geometry. This study characterizes the tool wear through measuring and comparing four anvils at different wear stages with a high-resolution metrology system. In addition, tool wear formation is investigated by using high-speed imaging to analyze the relative vibration of the metal sheets and tools during welding. Finally the relationship between tool condition and online monitoring signals is established using statistical models and an online model updating scheme is proposed under the Bayesian framework.*

## 1. Introduction

In manufacturing lithium-ion battery packs for electrical vehicles such as the Chevy Volt, it is critical to create reliable interconnections between battery cells, module-to-module, and module-to-control unit. Such joint connections must possess reliable electrical conductivity and sufficient mechanical strength to ensure battery performance. Ultrasonic metal welding has been adopted for battery tab joining in lithium-ion battery pack manufacturing due to its advantages in joining dissimilar and conductive materials [1].

Ultrasonic metal welding is a solid-state joining process which uses ultrasonic vibration to generate oscillating shears between metal sheets clamped under pressure [2]. A typical ultrasonic metal welding system is shown in Fig. 1. It is reported that welding tool replacement is a major production cost in vehicle battery production. Specifically, the high production costs due to tool replacement and maintenance can be divided into three major categories [3]: (1) costs due to machine down-time; (2) costs for fabricating, reworking, or refurbishing the replaced tool elements; and (3) costs for removing worn tools and installing new tools before and after tool replacement.

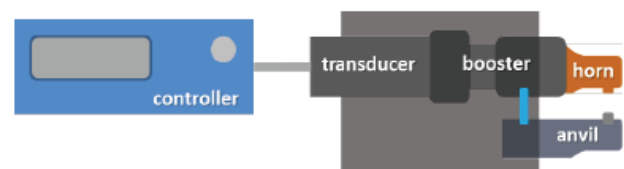


Fig. 1 A typical ultrasonic metal welding system [2]

Tool condition monitoring (TCM) is critically needed in automated manufacturing processes for the following reasons [4]:

- Automated high volume production cannot be sustained without an effective means for tool wear monitoring and tool breakage detection;
- Tool wear significantly affects production process operation, and thus should be closely monitored to guarantee consistent product quality. Tool condition information is essentially needed for accurate and adaptive quality monitoring;
- The benefits of economically using tool life cannot be achieved without a means for tool wear monitoring as a result of inevitable variations in tool life.

As a result, TCM has received tremendous attention over the past several decades. The majority of the TCM literature

has been focused on machining processes [4–17] and forming processes [3, 18–21]. Tool wear in turning and drilling processes have been studied most often. Some early studies investigated the mechanisms of tool wear for establishing various physical or empirical models (e.g., [5, 6]) and developing effective methods for tool wear monitoring [4, 7–14]. In general, tool wear monitoring techniques can be categorized into direct and indirect methods [15]. Direct methods measure the wear of the tools using visual inspection or computer vision etc. Indirect methods generally apply some sensors to collect process information and then estimate tool conditions using on-line signals. For direct tool wear monitoring, computer vision is the most popular technique [12–14]. However, direct methods have not always proven to be attractive economically or technically [4]. Therefore, indirect methods using on-line signals are often more desirable, as some exemplary scenarios in [4, 6–11]. A typical method for developing an indirect monitoring system include the following key steps [7]: (i) sensor selection, (ii) signal pre-processing, (iii) monitoring feature generation; (iv) feature selection/extraction; (v) monitoring decision and faulty classification using artificial intelligence technique. A thorough review on indirect monitoring methods can be found in [7]. TCM in micro-milling processes have also been studied in recent years [16, 17] utilizing similar monitoring methods as those applied to traditional cutting processes, such as hidden Markov models and neuro-fuzzy methods.

Additionally, tool wear in forming processes has also attracted some attention, especially extrusion and forging processes [3, 18–21]. Archard's wear model is widely applied in studies on extrusion processes [18, 19]. Statistical process control analysis of the tool wear evolution in a metal extrusion process was conducted in [20], which was used to identify the principal causes that result in the wear variability. On the TCM of forging processes, an on-line TCM system using artificial neural network to integrate information from multiple sensors was developed in [21].

Despite extensive literature discussing TCM for machining and forming processes, limited studies have been conducted on TCM of ultrasonic metal welding. There are several challenges in the development of a TCM system for ultrasonic metal welding. Firstly, only a limited understanding of the working mechanism of this process is available. Secondly, the tool wear development mechanism is not yet understood. Moreover, the geometry of welding tools, i.e., horn and anvil, is much more complicated than machining/forming tools. Fig. 2 shows sample knurl images on a horn and an anvil. There are a number of knurls on the tool surface. The knurl may take on different forms, such as that of a pyramid or semi-sphere. For a pyramid shaped knurl as shown in the figure, the knurl diagonal is between 1 mm and 2 mm, and the knurl height is several hundred microns, which can be difficult to measure using conventional computer vision systems. Thus, a high-resolution metrology system is necessary for tool wear characterization.

This paper presents some fundamental findings on the tool wear development and a preliminary method for tool condition monitoring for ultrasonic metal welding. Tool wear is depicted by utilizing a high-resolution metrology system to measure and compare the surface profiles of four anvils at different stages of wear. Tool wear development is investigated by

using high-speed imaging to analyze the relative vibration amplitudes between the metal sheets and tools during welding. To develop an online TCM algorithm for ultrasonic metal welding process, the relationship between tool condition and online monitoring signals is studied using regression and time series models with the Bayesian analysis framework.

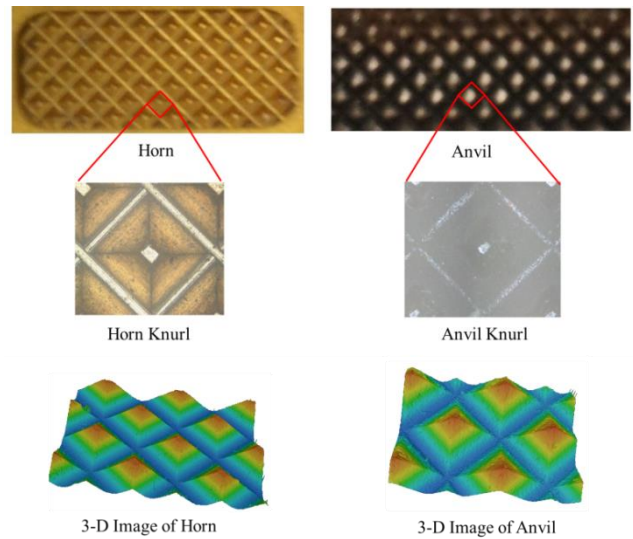


**Fig. 2 Tool geometry of ultrasonic metal welding.**

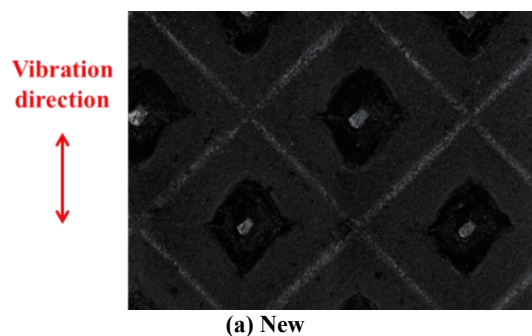
The remainder of this paper is organized as follows. Section 2 characterizes tool wear progression in ultrasonic welding based on high-resolution 3-D measurement. The tool wear mechanism is investigated in Section 3 using high speed imaging. Section 4 analyzes online monitoring signals and develops a tool condition monitoring algorithm. Section 5 concludes the paper.

## 2. Characterization of Tool Wear

This section presents the depiction of tool wear in ultrasonic metal welding based on height profile comparisons among anvils at different wear stages. For the sake of presentation simplicity, only results on anvil wear are shown in Fig. 3, which presents optical images of the anvils with the different shapes at the knurl level. Specifically, Subsections 2.1 and 2.2 present the wear progression patterns in the direction perpendicular to vibration and in the vibration direction, respectively.

### 2.1 Optical Images

Four anvils at different wear stages, i.e., new, half-worn, 3/4 worn, and worn, have been measured. Fig. 3 displays the optical images of typical knurls in these anvils.



**(a) New**

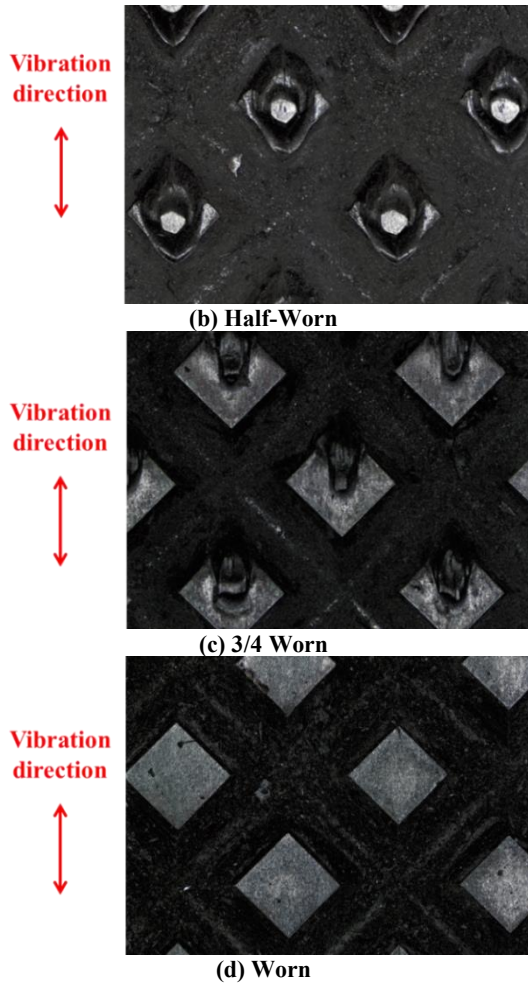


Fig. 3 Optical images of typical knurls in different anvils.

In Fig. 3(a), each knurl possesses regular a pyramid shape. However in Fig. 3(b), although the peaks remain in each knurl, the shapes are not as regular as in Fig. 3(a), where more materials have been removed at the left and right sides. Also materials have been lost at the upper and lower sides. In addition, the colors of peaks become shining after a certain number of welds, indicating wear. In Fig. 3(c), the left and right sides of each knurl are almost flat, and only a small amount of materials remain in the upper side. Finally in Fig. 3(d), all peaks have been removed and the knurls become completely flat.

**2.2 Tool Wear Progression in Direction Perpendicular to Vibration**

This subsection characterizes the wear progression in the direction perpendicular to the vibration, as shown in Fig. 3. In each anvil, one measurement is conducted in the cross section to display the height profiles of eight knurls, and the results are presented in Fig. 4, which clearly shows how wear develops.

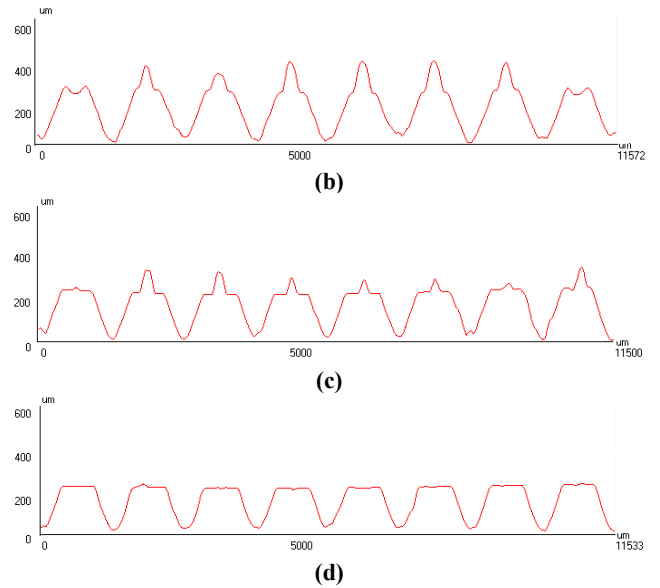
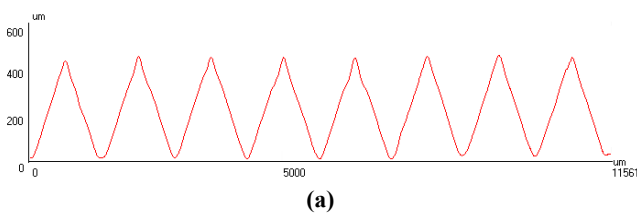
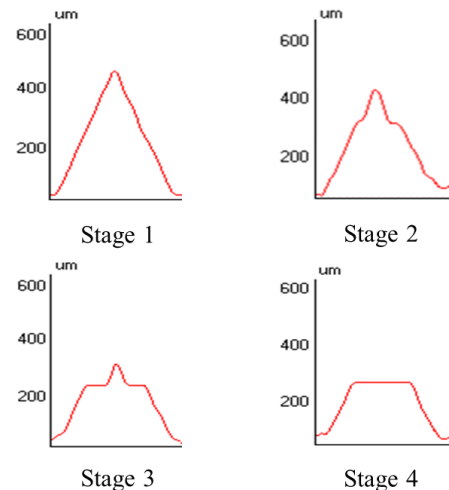


Fig. 4 Height profiles in the direction perpendicular to vibration.

In Fig. 4(a), one can see that the cross sections of all knurls of a new tool have triangle shapes and similar peak height. In Fig. 4(b), three types of tool wear patterns can be observed: (1) flank wear, (2) side wear, and (3) breakage. The flank wear is at the upright direction, which occurs with the removal of peaks (height decreases); the side wear represents the wear around the peaks, where two “shoulders” form at the left and right sides; the breakage usually happens from the center of weld area, which is indicated by a depressed shape. In Fig. 4(c), the height reduces significantly compared with Fig. 4(b), and some of the peaks are almost removed. Additionally, the width of shoulders increases. In Fig. 4(d), all peaks have disappeared, and the surface becomes completely flat, indicating breakage of the knurls.

Based on the findings revealed by Fig. 4, the knurl wear progression can be divided into four stages, as illustrated by Fig. 5, which are summarized as follows:

- Stage 1: The knurl is new, and it possesses a triangle shape.
- Stage 2: Material is removed in both downward and lateral directions, and shoulders appear on the left and right sides.
- Stage 3: Height decreases significantly, and the width of shoulders increases.
- Stage 4: Material is removed until the peak disappears, and the surface becomes completely flat.



**Fig. 5 Anvil knurl wear progression in the direction perpendicular to vibration.**

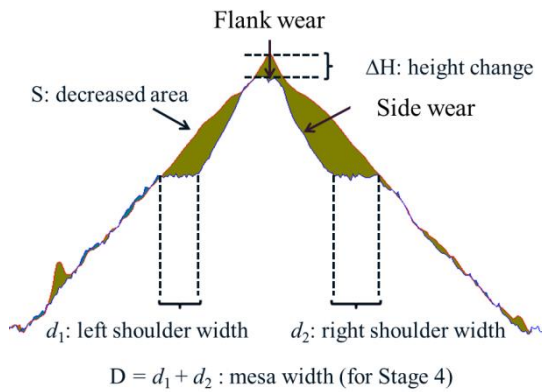


**Fig. 6 Proposed features for wear quantification in the direction perpendicular to vibration.**

To quantify the wear level, several profile features are proposed as shown in Fig. 6.  $\Delta H$  represents the decrease amount of the peak height;  $S$  is the decrease amount of the side areas;  $d_1$  and  $d_2$  are the width of the left and right shoulders, respectively, and when the knurl reaches Stage 4, they will be replaced by one feature,  $d$ , which is the length of the flat area.

It should be noted that some of the proposed features may be redundant; thus, further analysis is needed for feature selection.

**2.3 Tool Wear Progression in Vibration Direction**

Similar to Subsection 2.2, we measure the aforementioned four anvils in the direction parallel to the vibration, as shown in Fig. 3, and the results are shown in Fig. 7.

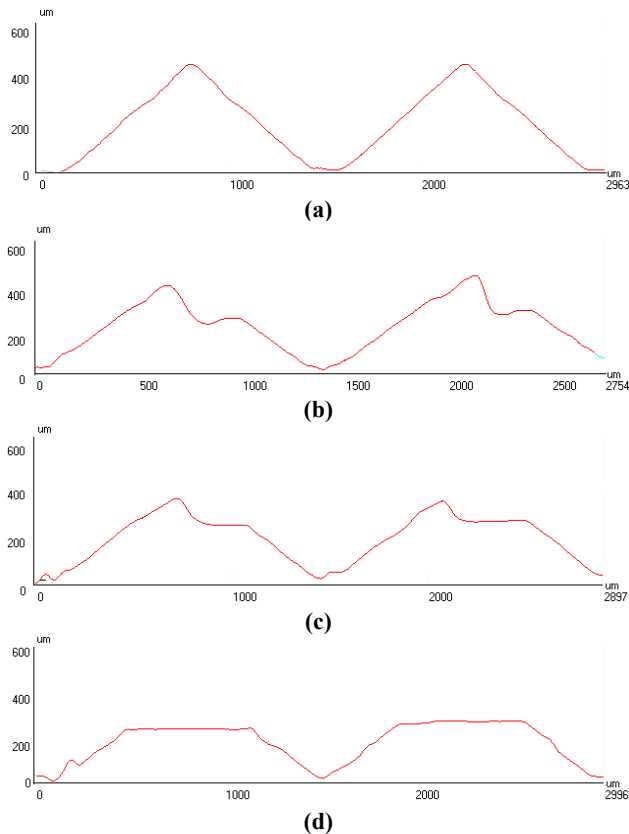
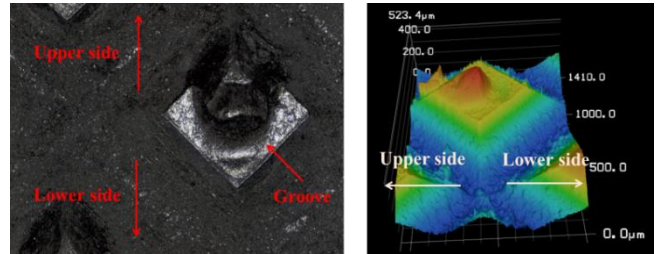


**Fig. 7 Height profiles in the vibration direction.**

As shown in Fig. 7 (a), a new anvil has triangle shapes. In Fig. 7 (b), an asymmetric pattern can be seen in two sides of the knurl in the vibration direction: more materials have been removed in the knurl's lower side in Fig. 3(b), and a groove appears. A knurl in this stage has two peaks, i.e., a main peak and a side peak. This asymmetry is further illustrated in Fig. 8. Fig. 8 (a) is an optical image obtained by a microscope, and Fig. 8 (b) is a 3-D image.



**(a) Optical image (b) 3-D image**  
**Fig. 8 Asymmetry wear progression pattern in the vibration direction.**

In Fig. 7 (c), one can see that after more material removal, the side peak in Fig. 7 (b) disappears and only a main peak remains. Fig. 7 (d) shows the final wear stage in the vibration direction. The main peak in Fig. 7 (c) has been completely removed, and a flat surface forms in the end.

According to the results shown in Fig. 7, the wear progression in the vibration direction is divided into four stages as illustrated by Fig. 9. The stages are summarized as follows:

*Stage 1:* The knurl is new, and it possesses a triangle shape.

*Stage 2:* Materials are mainly removed in the lower side, where a groove and a side peak form. The height of the main peak decreases compared with Stage 1.

*Stage 3:* More materials are removed until the side peak disappears. The height of the main peak continually decreases.

*Stage 4:* Finally, the main peak is completely removed, and the surface becomes flat.

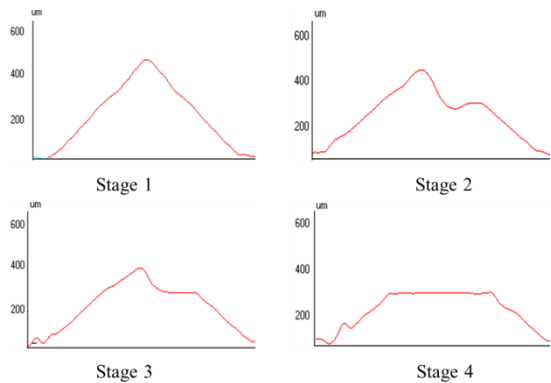


**Fig. 9 Anvil knurl wear progression in the vibration direction.**

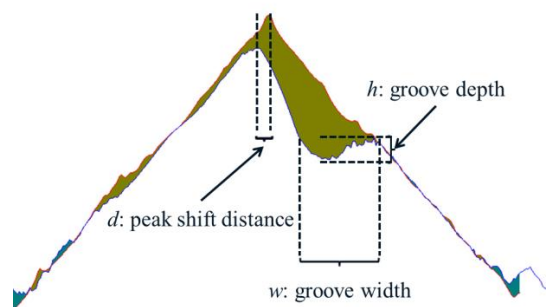


**Fig. 10 Proposed features for wear quantification in the vibration direction.**

To quantify the wear level, several features are proposed as shown in Fig. 10.  $d$  is the amount of the peak shift;  $h$  and  $w$  are the depth and width of the groove. Note that feature selection is needed to choose the best subset of features.

### 3. Tool Wear Mechanism

In this section, high-speed imaging is utilized to analyze the vibration behavior of each metal layer during welding, and the wear mechanism is then explained based on the analysis.

#### 3.1 Experimental Setup

High-speed imaging has been widely used to analyze various welding techniques, e.g., laser welding [22] and arc welding [23], but has never been attempted for ultrasonic metal welding due to its high frequency characteristics. However, recent development in high-speed imaging technology enables the observation of high frequency oscillations of the metal sheets in ultrasonic welding.

A Phantom v1610 digital high-speed camera with a telescope lens was used to record the dynamics of the metal workpiece during ultrasonic welding. Three layers of 0.2 mm nickel-plated C11000 copper (top) and one layer of the same material but 1.0 mm (bottom) were placed on an anvil. Fig. 11(a) illustrates the side view of the camera setup showing the workpiece aligned with the horn. This alignment was intended to observe the vibration behavior of the horn and workpiece together.

The images were taken at 100,000 frames per second with an exposure time of 9  $\mu$ s, which provides five images per one vibration cycle. The size of the image was  $256 \times 256$  pixels. The small vibration motion of a metal layer, tens of microns, was able to be recorded owing to a 35 times zoom capability of the telescope lens together with the CCD. Light was provided by a 150W Dolan-Jenner illuminator through fiber optic light-guides for high-speed imaging. Finally, the images were digitally obtained and processed by Phantom camera control application software. The lateral displacement of each metal layer was measured in the consecutive high-speed images as illustrated in Fig. 11(b).

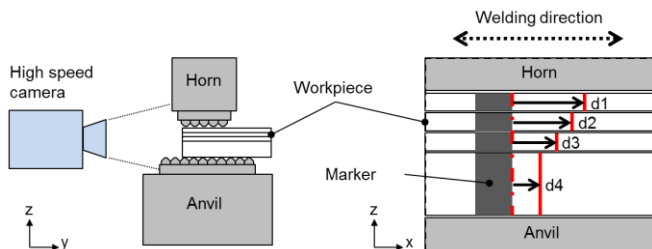


**Fig. 11 Schematic of high-speed camera setup: (a) workpiece stack-up aligned with horn (side view); and (b) displacement measurement of metal layer (front view) [24]**

The metal sheets were welded by a 20 kHz, 3.6 kW, *AmTech* lateral-drive ultrasonic spot welder. The clamping pressure, the horn vibration amplitude, and the weld time were chosen as 50 psi, 60  $\mu$ m, and 0.4s, respectively.

#### 3.2 Tool Wear Formation

To show the variations of lateral movements of the metal layers, the vibration magnitudes at different weld times are

obtained and plotted against time as described in Fig. 12.

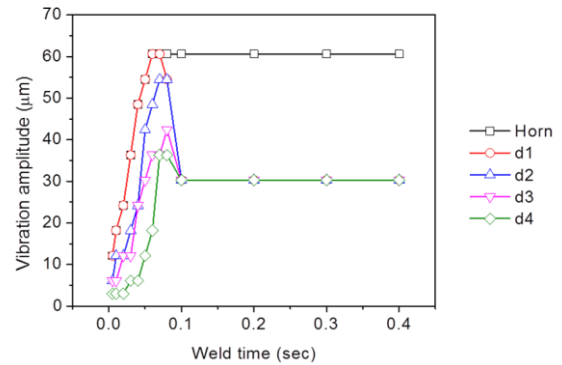


**Fig. 12 Progress of vibration amplitude of horn and four metal layers during the entire welding process [24]**

From Fig. 12 one can see that at the beginning of the weld cycle, each layer vibrates at a different amplitude which changes over time. After some time, all the vibrations converge into the same amplitude for the rest of the welding process. Specifically,

- Up to 0.1s, the vibration amplitudes of all four layers are different and then converge at 30  $\mu$ m and stay until the end of the process.
- After 0.1s weld time, slippage is observed between the tool (both horn and anvil) and metal sheets since the horn is vibrating at a magnitude of 60  $\mu$ m and the anvil is stationary.

From Fig. 12, one can observe that during a short period after the weld began, the horn and the first metal layer had the same amplitude, but afterwards, they have different amplitudes. Especially after 0.1s, the vibration amplitude of the horn stayed at 60  $\mu$ m, and that of the first metal layer was 30  $\mu$ m. Therefore, sliding friction exists between the horn and the metal sheets, and this contributes to the horn wear.

On the other hand, the anvil was static during welding, and the vibration amplitude of the fourth layer increased from 0 after the weld started, and reached 30  $\mu$ m at 0.1 s. After 0.1 s, it stayed at 30  $\mu$ m until the end of the weld. Thus, there is always sliding friction between the fourth metal sheet and the anvil, and contributes to the anvil wear.

More detailed discussion on the real-time vibration behaviors of metal layers and welding tools in ultrasonic welding can be found in [24].

### 4. Tool Condition Monitoring Using Online Signals

In this section, the relationship between tool conditions and online signals is established using regression and time series models. Since the mechanism behind oscillation in ultrasonic metal welding is directly affected by the geometry of the tool, the actual vibration frequency during welding gives a good indication about tool conditions. The dominant frequency can be extracted from monitoring signals using the Fourier transform or can be directly collected from microphone.

Fig. 13 shows the dominant frequencies from high-quality welds produced in a four-month period. Anvil changes are

indicated by the red dashed lines. Among the 8 anvils used in this period, anvil #1, 3, 4, 5, 7, and 8 were used in more than 20,000 welds. In order to establish a model for the dominant frequency with respect to tool degradation, we consider the data from these 6 anvils for analysis.

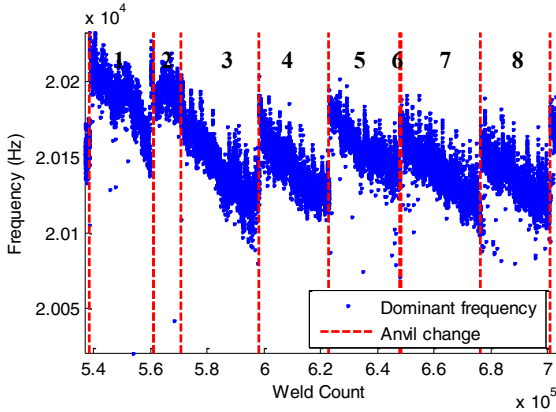


Fig. 13 Dominant frequencies and anvil changes.

#### 4.1 Relationship between Tool Conditions and Frequency Features

Denote the model response,  $y_i$ , to be the dominant frequency of the  $i$ th weld produced by the current anvil. The model predictor,  $X_i$ , is the number of welds produced by the current anvil so far. The relationship between  $y_i$  and  $X_i$  is established for each anvil. Among different anvils, the model parameters may be different but the model structure should be consistent.

The relationship between  $y_i$  and  $X_i$  is characterized by a linear model with autocorrelated and heteroscedastic residuals:

$$y_i = \beta_0 + \beta_1 X_i + \epsilon_i \quad (1)$$

$$\epsilon_i = c + \phi_1 \epsilon_{i-1} + u_i + \theta_1 u_{i-1} \quad (2)$$

$$u_i = \sigma_i v_i \quad (3)$$

$$\sigma_i^2 = \kappa + \alpha_1 u_{i-1}^2 + \gamma_1 \sigma_{i-1}^2 \quad (4)$$

where (2)–(4) represent a time series model for the residuals:

$$v_i \sim i. i. d. Normal(0,1)$$

$$u_i | \sigma_1^2, \dots, \sigma_{i-1}^2 \sim i. i. d. Normal(0, \sigma_i^2).$$

The model parameters can be estimated by a three-step method:

- i. Estimate the parameters in (1) by ordinary least squares (OLS):

$$\hat{\beta} = (X^T X)^{-1} X^T y$$

where

$$\beta = [\beta_0 \ \beta_1]^T, X = \begin{bmatrix} 1 & X_1 \\ \vdots & \vdots \\ 1 & X_N \end{bmatrix}, y = [y_1 \ \dots \ y_N]^T;$$

- ii. Fit model (2) - (4) to the OLS residuals  $\{\epsilon_i\}$  and estimate parameters.

Based on the Ljung-Box Q-test and Engle's test, we corroborated that the residuals  $\{\epsilon_i\}$  were autocorrelated and also conditional heteroscedastic. Hence, we introduced the autoregressive–moving-average (ARMA) model [25] to deal with conditional means and the generalized autoregressive conditional heteroscedastic (GARCH) model [26] to deal with variance heteroscedasticity. The degrees of the ARMA-GARCH model can be selected by the Bayesian information criterion (BIC). The above (2)–(4) represent an ARMA(1,1) – GARCH(1,1) model, which is determined without loss of generality.

- iii. Re-estimate the parameters in (1) using weighted least

squares (WLS):

$$\hat{\beta} = (X^T W X)^{-1} X^T W y \quad (5)$$

where the weights are the reciprocals of the conditional variances:  $W_{ii} = \frac{1}{\sigma_i^2}$  and  $\sigma_i^2$  is estimated by the GARCH(1,1) model.

To sum up the above three steps, the relationship between the dominant frequency ( $y_i$ ) and the number of welds produced by the current anvil ( $X_i$ ) can be represented by a linear model with ARMA-GARCH residuals.

Fig. 14 shows the dominant frequencies with the fitted lines given by model (1)–(5) for all 6 anvils analyzed. Table 1 gives the estimated model parameters for these anvils. Notice that the model parameters are slightly different for different anvils although the model structure is identical. This model structure provides in-depth information about historical anvils and also lays foundation for online tool condition monitoring and prediction.

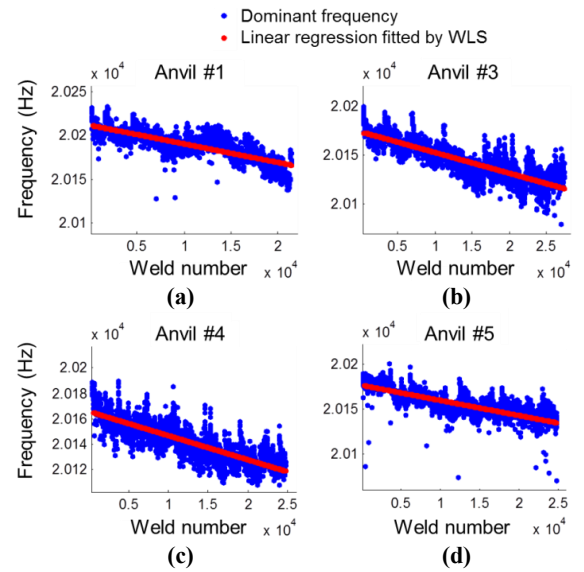


Fig. 14 Dominant frequencies and linear regression lines given by weighted least squares: (a) Anvil #1; (b) Anvil #3; (c) Anvil #4; (d) Anvil #5; (e) Anvil #7; and (f) Anvil #8.

Table 1. Model parameters.

	Anvil #1	Anvil #3	Anvil #4	Anvil #5	Anvil #7	Anvil #8
$\beta_0$	20212	20174	20166	20177	20161	20153
$\beta_1$	-	-	-	-	-	-
$c$	-0.008	0.000	-0.073	-0.025	-0.112	-0.003
$\phi_1$	0.978	0.967	0.955	0.969	0.942	0.944
$\theta_1$	-0.771	-0.717	-0.704	-0.756	-0.642	-0.708
$\kappa$	15.591	0.027	12.506	12.205	26.657	27.605
$\alpha_1$	0.075	0.012	0.095	0.124	0.120	0.142
$\gamma_1$	0.624	0.988	0.622	0.607	0.311	0.505

#### 4.2 Modeling for Online TCM

Since each anvil is unique, online tool condition monitoring should adjust the parameters for the current anvil instead of only adopting historical parameters given by Table 1. Hence, an updating scheme is needed in order to estimate and update the parameters of the model developed in Section 4.1. The model parameters are updated to reflect the uniqueness of the current anvil. The updated model is then used to predict feature values in future and estimate the remaining tool life. Fig. 15 illustrates the flowchart of online TCM and tool life

prediction.

During online TCM,  $n$  data points are observed at  $X_n$ ,  $n = 1, 2, \dots, N$ . Based on  $(X_1, y_1), \dots, (X_n, y_n)$ , a linear regression model with ARMA(1,1) – GARCH(1,1) residuals can be developed using the method in Section 4.1. Denote the set of all model parameters as  $\delta = (\beta_0, \beta_1, c, \phi_1, \theta_1, \kappa, \alpha_1, \gamma_1)$ .  $\delta$  is then updated through Bayesian estimation. The posterior mean values of  $\delta$  are then used to predict future values  $y_{n+1}, y_{n+2}, \dots$  and estimate the remaining tool life.

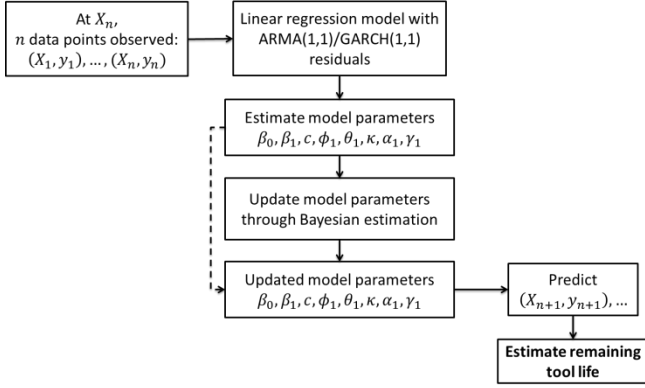


Fig. 15 Flowchart of online TCM and prediction.

To perform Bayesian analyses of the linear and ARMA-GARCH model given in model (1) – (5), we construct the posterior density function of the model:

$$p(\delta|y, X) = \frac{l(y|X, \delta)p(\delta)}{\int l(y|X, \delta)p(\delta)d\delta} \quad (6)$$

where  $\delta$  is the set of all parameters in the ARMA-GARCH model,  $l(y|X, \delta)$  is the likelihood function, and  $p(\delta)$  is the prior. The likelihood function of the ARMA-GARCH model is

$$l(y|X, \delta) = \prod_{i=1}^n \frac{1}{\sqrt{2\pi\sigma_i^2}} \exp\left[-\frac{\hat{u}_i^2}{2\sigma_i^2}\right] \quad (7)$$

where

$$u_i = \begin{cases} u_0 & (i = 0) \\ y_i - \beta_0 - \beta_1 X_i - c - \phi_1 (y_{i-1} - \beta_0 - \beta_1 X_{i-1}) - \theta_1 u_{i-1} & (i = 1, \dots, n) \end{cases} \quad (8)$$

and we assume  $y_0 = \beta_0, X_0 = 0$  as starting values.

For the prior, we use the following proper prior:

$$p(\delta) = N(\mu_{\beta_0}, \Sigma_{\beta_0}) \times N(\mu_{\beta_1}, \Sigma_{\beta_1}) \\ \times N(\mu_{c, \phi_1}, \Sigma_{c, \phi_1}) I_{C1}(c, \phi_1) \times N(\mu_{\theta_1}, \Sigma_{\theta_1}) I_{C1}(\theta_1) \\ \times N(\mu_{\kappa, \alpha_1}, \Sigma_{\kappa, \alpha_1}) I_{C2}(\kappa, \alpha_1) \times N(\mu_{\gamma_1}, \Sigma_{\gamma_1}) I_{C2}(\gamma_1) \quad (9)$$

where  $I_{C1}(\cdot)$  and  $I_{C2}(\cdot)$  are indicator functions which take unity if the constraints hold, and  $N(\cdot)$  represents the normal distribution. C1 is the constraint related to the stationarity and invertibility of the ARMA process, and C2 is imposed to guarantee that the conditional variance  $\sigma_i^2$  is always positive.

The posterior distributions of parameters in the ARMA-GARCH model are approximated by the Gibbs sampler. The Gibbs sampler algorithm iteratively generates a dependent sequence of parameters  $\{\delta^{(1)}, \delta^{(2)}, \dots, \delta^{(S)}\}$ . The median of  $\{\delta^{(1)}, \delta^{(2)}, \dots, \delta^{(S)}\}$  is then used as the updated parameters for online TCM and prediction.

During online TCM, model parameters  $\delta$  are estimated at  $X_n$  and then updated through Bayesian analysis and Gibbs sampling algorithm. The posterior values of  $\delta$  are then used to predict future values  $y_{n+1}, y_{n+2}, \dots$  and estimate the remaining tool life. Fig. 16 shows the prediction of feature values  $y_{n+1}, y_{n+2}, \dots$  for anvil #7 at  $n = 600, 1000, 1500,$  and  $2000$ . The light blue dots are observed

feature values till  $X_n$ ; the blue line is the fitted linear regression model with ARMA-GARCH residuals based on Section 4.1; the grey dots are true feature values after  $X_n$ ; the red line and black dashed lines are the predicted mean feature values and confidence intervals at  $\alpha = 0.05$ , respectively.

As can be seen from Fig. 16, the prediction is adjusted when more observations become available. The newly observed feature values reflect not only the general production condition, but also actions occurred in this period, such as tool cleaning. The updating scheme is executed automatically to consider the changes brought by the new observations and then to adjust the predicted trend accordingly.

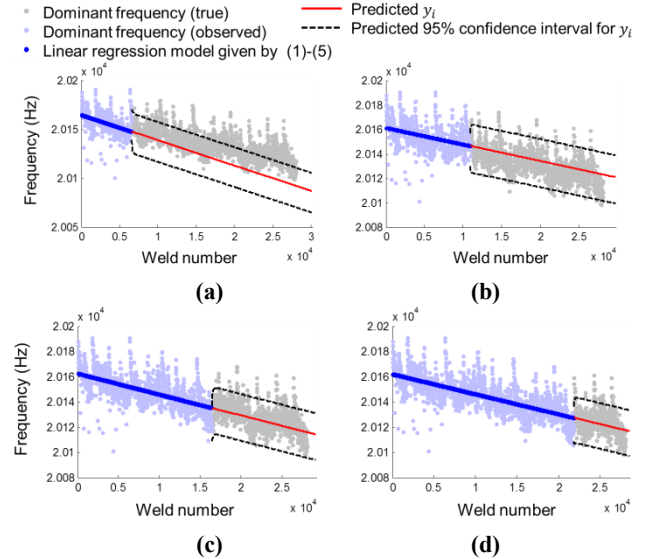


Fig. 16 Prediction of feature values (anvil #7) at (a)  $n=600$ ; (b)  $n=1000$ ; (c)  $n=1500$ ; and (d)  $n=2000$ .

The remaining anvil life can be estimated based on the predicted feature values when an anvil life threshold is known. The threshold can be approximated based on the prior knowledge of the remaining tool life (in terms of a percentage or number of welds) of these historical anvils (anvil #1, 3, 4, 5, and 7).

## 5. Conclusions and Future Work

In this study, some preliminary results on the characterization and monitoring of tool wear in ultrasonic metal welding have been presented. More specifically, three topics were discussed:

- (1) Wear progression in anvil knurl has been depicted in two directions, i.e., the direction perpendicular to vibration and the vibration direction, by comparing height profiles of anvils at different wear stages. The knurl wear can be divided into four stages, and different wear patterns exist in two directions.
- (2) Tool wear mechanism has been explained by measuring the vibration amplitudes of horn and metal layers during welding. Sliding friction induced by relative displacements contributes to the wear of horn and anvil.
- (3) The relationship between the anvil conditions and the features extracted from online signals has been established using the regression and time series models.

More research work is needed to develop an effective TCM system for ultrasonic metal welding, and our ongoing

efforts have been focused on:

- (1) Characterizing the tool wear in anvil/horn level, and finding the best representative features to quantify tool wear.
- (2) Improving the TCM model such that it can be robust to the inevitable noises in the on-line monitoring features.

## ACKNOWLEDGEMENT

This material is based upon work supported by the Department of Energy under Award Number DE-EE0002217.

## DISCLAIMER

This paper was prepared as an account of work sponsored by an agency of the United States Government. Neither the United States Government nor any agency thereof, nor any of their employees, makes any warranty, express or implied, or assumes any legal liability or responsibility for the accuracy, completeness, or usefulness of any information, apparatus, product, or process disclosed, or represents that its use would not infringe privately owned rights. Reference herein to any specific commercial product, process, or service by trade name, trademark, manufacturer, or otherwise does not necessarily constitute or imply its endorsement, recommendation, or favoring by the United States Government or any agency thereof. The views and opinions of authors expressed herein do not necessarily state or reflect those of the United States Government or any agency thereof.

## REFERENCES

1. Kim, T. H., Yum, J., Hu, S. J., Spicer, J. P., and Abell, J. A. (2011). Process robustness of single lap ultrasonic welding of thin, dissimilar materials. *CIRP Annals-Manufacturing Technology*, 60(1), 17–20.
2. Shao, C., Paynabar, K., Kim, T. H., Jin, J. J., Hu, S. J., Spicer, J. P., and Abell, J. A. (in press). Feature selection for manufacturing process monitoring using cross-validation. *Journal of Manufacturing Systems*, 32(4), 550–555.
3. Lange, K., Cser, L., Geiger, M., and Kals, J. A. G. (1992). Tool life and tool quality in bulk metal forming. *CIRP Annals-Manufacturing Technology*, 41(2), 667–675.
4. Jantunen, E. (2002). A summary of methods applied to tool condition monitoring in drilling. *International Journal of Machine Tools and Manufacture*, 42(9), 997–1010.
5. Cook, N. H. (1973). Tool wear and tool life. *Journal of Engineering for Industry*, 95, 931.
6. Koren, Y., Ko, T.-R., Ulsoy, A. G., and Danai, K. (1991). Flank wear estimation under varying cutting conditions. *Journal of Dynamic Systems, Measurement, and Control*, 113.2, 300–307.
7. Abellan-Nebot, J. V., and Subirón, F. R. (2010). A review of machining monitoring systems based on artificial intelligence process models. *The International Journal of Advanced Manufacturing Technology*, 47(1–4), 237–257.
8. Rehorn, A. G., Jiang, J., and Orban, P. E. (2005). State-of-the-art methods and results in tool condition monitoring: a review. *The International Journal of Advanced Manufacturing Technology*, 26(7–8), 693–710.
9. Zhou, J. H., Pang, C. K., Zhong, Z. W., and Lewis, F. L. (2011). Tool wear monitoring using acoustic emissions by dominant-feature identification. *IEEE Transactions on Instrumentation and Measurement*, 60(2), 547–559.
10. Ertunc, H. M., Loparo, K. A., and Ocak, H. (2001). Tool wear condition monitoring in drilling operations using hidden Markov models (HMMs). *International Journal of Machine Tools and Manufacture*, 41(9), 1363–1384.
11. Snr, D., and Dimla, E. (2000). Sensor signals for tool-wear monitoring in metal cutting operations—a review of methods. *International Journal of Machine Tools and Manufacture*, 40(8), 1073–1098.
12. Kurada, S., and Bradley, C. (1997). A review of machine vision sensors for tool condition monitoring. *Computers in Industry*, 34(1), 55–72.
13. Kurada, S., and Bradley, C. (1997). A machine vision system for tool wear assessment. *Tribology International*, 30(4), 295–304.
14. Lanzetta, M. (2001). A new flexible high-resolution vision sensor for tool condition monitoring. *Journal of Materials Processing Technology*, 119(1), 73–82.
15. Byrne, G., Dornfeld, D., Inasaki, I., Ketteler, G., König, W., and Teti, R. (1995). Tool condition monitoring (TCM)—the status of research and industrial application. *CIRP Annals-Manufacturing Technology*, 44(2), 541–567.
16. Zhu, K., Wong, Y. S., and Hong, G. S. (2009). Multi-category micro-milling tool wear monitoring with continuous hidden Markov models. *Mechanical Systems and Signal Processing*, 23(2), 547–560.
17. Malekian, M., Park, S. S., and Jun, M. B. (2009). Tool wear monitoring of micro-milling operations. *Journal of Materials Processing Technology*, 209(10), 4903–4914.
18. Kang, J. H., Park, I. W., Jae, J. S., and Kang, S. S. (1999). A study on a die wear model considering thermal softening: (I) Construction of the wear model. *Journal of Materials Processing Technology*, 96(1), 53–58.
19. Kang, J. H., Park, I. W., Jae, J. S., and Kang, S. S. (1999). A study on die wear model considering thermal softening (II): Application of the suggested wear model. *Journal of Materials Processing Technology*, 94(2), 183–188.
20. Lepadatu, D., Hambli, R., Kobi, A., and Barreau, A. (2006). Statistical investigation of die wear in metal extrusion processes. *The International Journal of Advanced Manufacturing Technology*, 28(3–4), 272–278.
21. Kong, L. X., and Nahavandi, S. (2002). On-line tool condition monitoring and control system in forging processes. *Journal of materials processing technology*, 125,

464–470.

22. Eriksson, I., Gren, P., Powell, J., and Kaplan, A. F. (2010). New high-speed photography technique for observation of fluid flow in laser welding. *Optical Engineering*, 49(10), 100503–100503.
23. Wen, Y. M., Huang, S. S., and Liu, G. X. (2011). Testing and Analysis of High-Speed Camera for Droplet Transition. *Advanced Materials Research*, 271, 79–83.
24. Lee, S (2013). Process and Quality Characterization for Ultrasonic Welding of Lithium-Ion Batteries. The University of Michigan.
25. Box, G. E. P., Jenkins, G. M., and Reinsel, G. C. (1994), *Time series analysis: forecasting and control. 3rd ed.*, Prentice Hall, Upper Saddle River, NJ.
26. Engle, R. F. (1982). Autoregressive conditional heteroscedasticity with estimates of the variance of United Kingdom inflation. *Econometrica: Journal of the Econometric Society*, 987–1007.